CHAPTER 1

Practical Approaches for In Situ *X-ray Crystallography: from High-throughput Screening to Serial Data Collection*

ISABELLE MARTIEL,[a] VINCENT OLIERIC,[a] MARTIN CAFFREY[b] AND MEITIAN WANG*[a]

[a] Swiss Light Source, Paul Scherrer Institute, CH-5232 Villigen, Switzerland; [b] Membrane Structural and Functional Biology Group, Schools of Medicine and Biochemistry and Immunology, Trinity College, Dublin, Ireland
*Email: meitian.wang@psi.ch

1.1 Introduction

1.1.1 What Exactly Is *In Situ*?

In macromolecular crystallography (MX), *in situ* data collection refers to a diffraction measurement performed on crystals where and as they grow. In other words, the crystals are not harvested individually from their growth environment, as is typically done in standard MX with a harvesting loop. Thus, in the *in situ* experiment, the original growth medium and the

Chemical Biology No. 8
Protein Crystallography: Challenges and Practical Solutions
Edited by Konstantinos Beis and Gwyndaf Evans

Published by the Royal Society of Chemistry, www.rsc.org

crystallization compartment remain in place surrounding the crystal during interrogation with the X-ray beam. By contrast, both are removed or minimized in classical loop harvesting protocols to increase diffraction signal-to-noise ratio (SNR) by minimizing background scattering. In the strictest embodiment of an *in situ* experiment, the crystal growth plate or chamber must remain hermetically sealed from the moment the crystallization experiment is set up and data collection must be done at growth temperature. However, many so-called *in situ* measurements are made under conditions departing to varying degrees from this limiting definition.

A few examples illustrate the extent to which the *in situ* label has been used. Jet sample delivery developed at X-ray free electron laser (XFEL) facilities has been considered an *in situ*-like method. In this case, microcrystals remain suspended in the mother liquor or the lipid cubic phase (LCP) where they grew. However, these samples have been transferred between syringes and reservoirs, sometimes filtered, and finally extruded under pressure into an X-ray chamber that is sometimes under vacuum. These post-growth handling steps accompanied by variations in pressure and temperature can mean that data is collected under conditions that are far removed from *in situ*. Several methods, sometimes presented as *in situ* methods, include a mother liquor removal step, such as the Crystal Direct approach[1] (see Section 1.2) and several XFEL solid support sample preparation methods, where the mother liquor is blotted[2] or sucked away[3] to help position crystals into ordered wells. This mother liquor removal distinguishes these preparation methods from *in situ* experiments.

In this chapter, after a general introduction to *in situ* experiments (Section 1.1), we will cover the different *in situ* setups and the evolution of the field, following a historical perspective. *In situ* experiments date back to the period where X-ray capillaries were used to grow crystals by microdialysis and interface diffusion methods, in order to avoid the difficulties of transferring grown crystals into capillaries for data collection.[4] However crystal movement in the capillary often made the technique impractical.[5] In the 1990s, García-Ruiz and coworkers formalized gel-acupuncture methods to collect data on *in situ* counter-diffusion grown crystals in capillaries without any post-growth transfer, at room temperature and under cryogenic conditions.[4,5] In 2004, Jacquamet, Ferrer and coworkers demonstrated the first *in situ* capable automated setup at a synchrotron beamline, where SBS-format crystallization plates were placed in the beam by a robot arm.[6] The automated handling of SBS-format plates has spread in many synchrotron facilities as well as to laboratory X-ray instruments since then (Section 1.2), benefiting in particular the field of virus crystallography.[7] An intense period of development of *in situ*-specific setups started in parallel, towards format reduction, microfluidic and on-chip systems (Section 1.3). The latest phase of development has seen the emergence of *in situ* experiments optimized for serial crystallography and compatible with data collection at cryogenic temperature (Section 1.4).

1.1.2 Goals of *In Situ* Experiments

In situ methods can be used for a variety of purposes at different stages of a project. In the phase of optimizing crystallization conditions, *in situ* screening can help distinguish between protein and salt or small molecule crystals, as a complement to UV fluorescence and second-order harmonic generation techniques.[8] The unique advantage of X-ray screening is the direct access to data collection-relevant information such as diffraction quality, space group and unit cell, which are not provided by optical techniques. *In situ* screening can therefore help to identify genuine protein crystal hits, to find the best diffracting crystal form in the case of polymorphs, or in the search of different space groups,[9] and to diagnose for loss of diffraction quality due to crystal manipulation and/or cryo-cooling. *In situ* screening can help increase the efficiency of the protein-to-structure pipeline by enabling diffraction-based identification of best conditions and ligand binding state. This is especially valuable for drug discovery applications involving ligand screening.[10,11]

In situ experiments are not limited to screening and optimization. In some projects they are used for final data collection and structure solution. This is the case for crystals that cannot be handled with a loop (crystal degradation upon opening of the well or during harvesting) or flash-cooled in liquid nitrogen, *e.g.* in virus crystallography,[7] or for very small crystals, such as virus and *in meso*-grown membrane protein crystals, where harvesting hundreds of crystals for serial crystallography is time-consuming and may not be practical (see Section 1.4). Due to limitations in the tolerable X-ray dose at room temperature and geometrical constraints imposed by some crystallization containers, it is almost impossible to collect a complete data set from a single crystal in certain *in situ* setups, as is usually done in standard cryo-crystallography. Accordingly, partial data sets from several crystals must be combined as practiced in micro- and serial crystallography.[12] Depending on the sample type, data collection can be performed either using a multi-crystal approach or using serial crystallography methods.[13] In the multi-crystal approach, a few partial data sets covering significant angular wedges from a few crystals are merged together. The sorting and merging of data sets are generally performed manually or semi-manually by the crystallographer. In the serial approach, large numbers of small wedges or even still images from many crystals are assembled, which requires automation in data set processing, selection and merging. The serial approach derives from serial femtosecond crystallography (SFX) data collection, where only still images are collected on thousands of randomly oriented small crystals.[14,15] In synchrotron-based serial data collection, wedges of typically a few degrees are collected on each crystal. In both cases, data collection of a complete data set relies on the varied or random orientation of crystals for adequate sampling of reciprocal space. Preferential orientation of the crystals on the plate or well surface is therefore to be minimized or compensated for by tilting the sample support during X-ray data collection.

With *in situ* methods, unnecessary manipulation of crystals by harvesting is avoided. However, harvesting is not always detrimental: clear cases where post-growth treatments such as dehydration increase the diffracting quality have been reported.[16] Methods for controlled dehydration and other post-growth treatments in *in situ* plates have been developed.[17] Another characteristic of manual harvesting is the introduction of a possible source of irreproducibility in the experiment, since two crystals are rarely harvested exactly in the same way, even by the same person. This is less of an issue with *in situ* methods.

Historically, *in situ* measurements are performed mainly at room temperature (RT) (see Section 1.2). RT data collection is often deemed biologically more relevant. Further, it enables the probing of conformational landscapes, time-resolved studies and chemical reactions in the crystals. Measurements at RT usually result in lower crystal mosaicity. In certain cases, such as with virus crystals, RT data collection is the only option due to crystal fragility and sensitivity to cryo-cooling. Recent developments with thin-film samples (see Section 1.4.1) offer the possibility to perform flash-cooling of *in situ* samples and to collect data under cryogenic conditions. Cryo-treatment is not compliant with the strict definition of *in situ*, but low temperature (100 K) data collection has significant advantages that include a 50- to 100-fold increase of the tolerable dose. Further, cryo-cooled samples are easily stored and transported.

1.1.3 Challenges of *In Situ* Methods

Here we list the challenges related to *in situ* experiments, of which users should be aware when selecting a particular method and planning experiments. The first and foremost challenge is the relatively high scattering background arising from the support and the growth medium surrounding the crystal. This generally results in sharp or diffuse scattering rings or arcs at intermediate-to-low scattering angles (~3–6 Å). Although *in situ* setups are usually optimized to reduce such scatter (see Section 1.1.4), background contribution will remain larger for most *in situ* setups compared to a correctly loop-harvested cryo-cooled crystal.

The second challenge, radiation damage, is not specific to *in situ* experiments. Detecting and managing radiation damage is also crucial for successful data collection with conventional methods.[18] With *in situ* methods, the problem of radiation damage is pronounced when data collection is done at RT and/or with small crystals. At RT, the tolerable dose per crystal is of the order of a fraction of a MGy,[19] while under cryogenic conditions at 100 K a single crystal can take up to about 20 MGy (the so-called Henderson limit[20,21]) for molecular replacement methods, or about 5 MGy for experimental phasing methods.[22] In practice, these should be considered as upper dose limits, since many crystals are more sensitive,[23] in a manner that depends on heavy atom content, crystal composition and crystallization conditions.

The third issue is the geometrical constraints imposed by *in situ* plates and supports, which limit the angular range of data that can be collected. The accessible angles vary with the type of plate and the setup. With some plates it is difficult to accurately position the beam on the crystals due to optical refraction by curved or thick plastic surfaces, and/or on the crystallization drops.[24] For this reason, plates with flat surfaces are preferred especially for small crystals, although they are not always convenient when surface active agents, such as detergents, are present in the crystallization conditions.

Special beamline equipment is necessary to perform most *in situ* measurements. Thus, suitable hardware to transport the plate or support into the beam and bespoke software must be available. Synchrotron facilities often have at least one beamline equipped for *in situ* experiments (Table 1.1). Serial crystallography approaches also require specific data acquisition, processing and merging software to handle the data. It is recommended to process and merge the data online, to monitor and optimize data quality and completeness during data collection.[24]

Since *in situ* methods are at the interface between crystallization and crystallography, several crystallization-related constraints should also be considered in the choice or design of the *in situ* setup. Thinner windows will enable faster evaporation of solvent from solutions inside the plates, such that the drops dry quicker.[25] Overcoming this issue for crystallization experiments that last for weeks requires either a compromise on the film thickness, a double-sandwich type setup to prevent evaporation (see Section 1.4.1), or a humidified plate storage environment. Special lids have also been designed to slow down evaporation.[25] Another point to consider is the compatibility with optical imaging systems (polarized light microscopy, UV fluorescence) to identify crystal hits, and with laboratory liquid handling robotics to set up the drops. Finally, one should bear in mind the influence of interfaces, geometry and drop size on nucleation probabilities and growth processes.[26] Optimization of crystallization conditions for a given type of plate or support is often required.

1.1.4 Enabling Technologies

The success of *in situ* crystallography has been facilitated by the introduction of a number of other technologies. Progress in synchrotron radiation technologies and X-ray optics has led to the introduction of microbeams[12,24] with a high flux density to address ever smaller crystals. The development of fast detectors, such as the PILATUS and EIGER detectors, enabled continuous data collection with weakly diffracting crystals.[34] Specific hardware has been developed to place *in situ* supports in the beam (Section 1.2). Beamline controls and software deliver a high level of automation, first introduced as an integrated setup at beamline BM30-FIP,[35,36] extending now to the fully automated MASSIF-1 beamline at the European Synchrotron Radiation Facility (ESRF).[37] Grid-scan or rastering procedures facilitate localizing

Table 1.1 *In situ* measurement capabilities reported at various synchrotron facilities.

Synchrotron	Beamline	Reported *in situ* capacities	References
APS	SBC 19-ID	SBS: Goniometer	27, https://www.sbc.anl.gov/
APS	GM/CA 23ID-B & D	Thin-film sandwich	28, http://www.gmca.anl.gov/
BESSY II	BL14.1	SBS: MD2 goniometer	29, https://www.helmholtz-berlin.de/forschung/oe/np/gmx/ancillary-facilities/insitu-screening_en.html
DLS	I03	SBS: Goniometer	http://www.diamond.ac.uk/Beamlines/Mx/Equipment-on-Demand/In-situ-Data-Collection.html
DLS	I24	SBS: Horizontal goniometer Thin-film sandwich: on vertical goniometer	http://www.diamond.ac.uk/Beamlines/Mx/Equipment-on-Demand/In-situ-Data-Collection.html
DLS	VMXi	SBS: Goniometer	http://www.diamond.ac.uk/Beamlines/Mx/VMXi.html
ESRF/FIP	BM30	SBS: G-rob robot	6, http://www.fip-bm30a.fr/index.php/trading-hours-and-holidays/manage-diaries/description/10-services-available-on-fip
ESRF/EMBL	ID30B	SBS: Goniometer	http://www.esrf.eu/id30b
ESRF	ID13	LCP jet	30, http://www.esrf.eu/UsersAndScience/Experiments/XNP/ID13
KEK	Several beamlines	SBS: Goniometer	31, http://www2.kek.jp/imss/sbrc/eng/beamline/px.html#beamline
LNLS	W01B-MX2	SBS: G-rob robot	http://lnls.cnpem.br/linhas-de-luz/mx2-en/overview/
MAX IV	BioMax	SBS: ISARA robot	https://www.maxiv.lu.se/accelerators-beamlines/beamlines/biomax/
NSLS II	FMX	SBS: Goniometer	https://www.bnl.gov/ps/beamlines/beamline.php?b=FMX
NSLS II	AMX	SBS: Goniometer	https://www.bnl.gov/ps/beamlines/beamline.php?b=AMX
PETRA III/EMBL	P14	SBS: Goniometer (CrystalDirect plates)	https://www.embl-hamburg.de/services/mx/P14/index.html
SLS	X06DA–PXIII	SBS: CATS robot	9, https://www.psi.ch/sls/pxiii/ https://www.psi.ch/sls/pxiii/crystallisation-facility
SLS	X06SA-PXI & X10SA-PXII	Thin-film sandwich LCP jet	11, 32, https://www.psi.ch/sls/pxi/
SOLEIL	PROXIMA1	SBS: CATS robot	http://www.synchrotron-soleil.fr/Recherche/LignesLumiere/PROXIMA1
Spring-8	BL32XU	Thin-film sandwich	33, https://beamline.harima.riken.jp/en/bl_info/bl32xu_info.html

crystals invisible by optical methods, identifying the best diffracting crystals or regions of crystals and performing diffraction-based crystal centering,[34,38] lately by an automated analysis of the rastering results.[39]

With regard to data processing and management, *in situ* data collection in crystallization plates has been facilitated enormously by powerful multi-crystal merging procedures. Crystal selection[40] and clustering methods[41,42] have also proven useful, as recently reviewed.[43] Data management of the often large number of crystallization trials has also received attention. The recent use of haptic interfaces is one such example.[44]

Early on, great effort was invested in optimizing the materials used to manufacture *in situ* plates and supports. The commercial availability of recently developed low background, UV-friendly specialty polymers, mainly cyclic olefin (co-)polymers, in industrial grades of suitable quality, thickness and affordability, has been integral to the success of the approach.[45] The design of new high-throughput *in situ* consumables often involves materials optimization and polymer processing. The success of a new *in situ* method is also often correlated to the translation into commercially available consumables, and the establishment of user-friendly, easily reproducible protocols.[11,32]

1.2 *In Situ* Screening at the Synchrotron: Standard SBS Plates

1.2.1 Development History

The first demonstration of automated *in situ* experiments on SBS-format plates, by Jean-Luc Ferrer and coworkers at the FIP-BM30A (French beamline for Investigation of Proteins) at the ESRF in 2004, opened a new paradigm for *in situ* experiments, inaugurating the era of high-throughput *in situ* methods. Jacquamet, Ferrer and coworkers[6] developed beamline hardware and software to perform *in situ* data collection directly in the crystallization plate in an easy and efficient manner (Figure 1.1). The SBS format for microplates was established around the year 2000 by the Society for Biomolecular Screening (SBS), now part of the Society for Laboratory Automation and Screening (SLAS), and the American National Standards Institute (ANSI). The goal was to ensure compatibility between plates from different manufacturers and laboratory automation instrumentation for drug discovery research. The 96-well SBS plates are therefore compatible with laboratory robotics used for drop setting in crystallization experiments and are now ubiquitous in crystallization laboratories. Although *in situ* experiments in SBS plates started mainly as a screening tool and are often called '*in situ* plate screening', the collection of complete data sets was performed early on, first on single high symmetry crystals[6] and then by merging data from a small number of crystals.[45] Serial-like data collection of small wedges from a large number of crystals was also later demonstrated.[46]

In situ data collection has been particularly beneficial in structural biology fields where crystals are fragile and difficult to flash-cool. For instance, virus

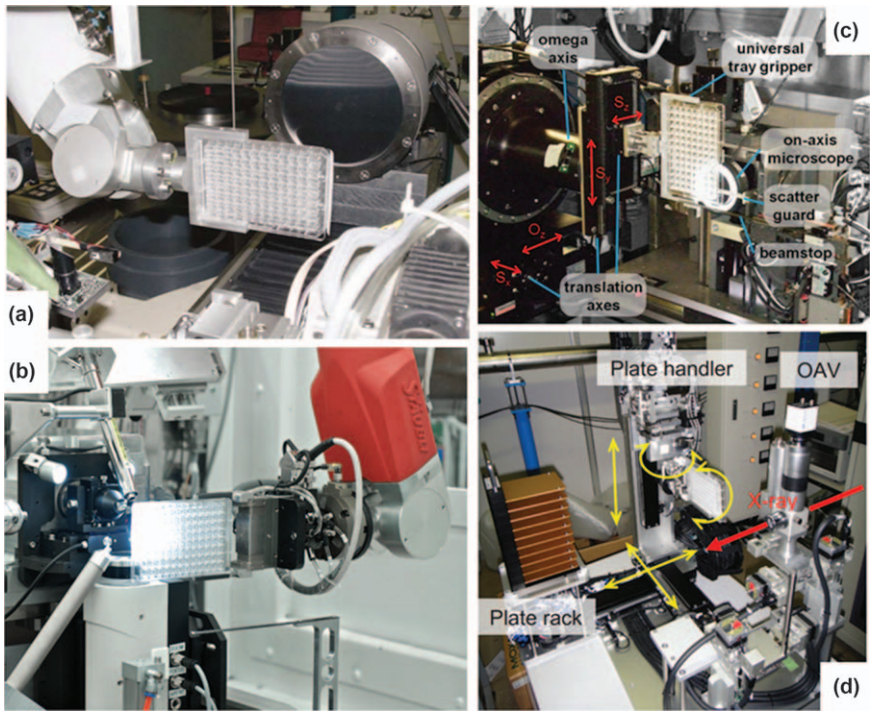

Figure 1.1 (a) The original plate screening setup at beamline FIP-BM30A (ESRF), reproduced from ref. 6. Copyright 2004, with permission from Elsevier.[6] (b) The CATS robot arm in position for data collection on a plate at beamline X06DA-PXIII (SLS), reproduced from ref. 9. Copyright 2011 American Chemical Society. (c) The I24 plate screening goniometer at the Diamond Light Source (DLS), reproduced under a Creative Commons License (https://creativecommons.org/licenses/by/2.0) from Axford *et al.*[24] Copyright 2012, International Union of Crystallography. (d) The PLEX system at the Photon Factory. Reprinted from ref. 31 with the permission of AIP Publishing.

crystals have large unit cells and weak crystal contacts and are notoriously fragile. It is often difficult to find suitable cryo-cooling conditions for such crystals, and the increase of mosaicity often observed upon cryo-cooling can result in spot overlap due to the large unit cell. For these reasons, most virus structures determined by X-ray crystallography are based on data collection at RT.[7,24,47]

Efforts are underway to make *in situ* plate experiments suitable for ligand screening applications. This includes fragment-based screening, which generally involves large numbers of crystals. Well-diffracting crystals are grown under identical crystallization conditions and are soaked (or co-crystallized) using a library of chemical ligands to determine the degree of binding. For fragment-based screening data set collection, high completeness and/or multiplicity is not always required.[45] Ligand addition for *in situ*-like ligand

screening experiments can be performed either using standard liquid handling robots[10] or by acoustic droplet ejection (ADE)[48] using, for example, the commercial system Labcyte Echo 550, or in-house built setups. The very small volumes (down to a few nanoliters) handled by ADE make it possible to multiply the number of crystallization or soaking trials and therefore to screen more ligands.[48] Gelin *et al.*[10] developed a method where the base of each well in the plate is coated with dry ligand. The ligand solubilizes in the dispensed crystallization drop and ideally diffuses into the crystal.

1.2.2 Plate Handling Hardware

Two types of plate handling hardware exist at beamlines for SBS plate *in situ* collection: robots and goniometers. An automatic sample changer robot, normally used to exchange cryo-cooled samples, can be equipped with a special gripper for moving SBS plates to and from a multi-plate hotel. The precision and stability of 6-axis industrial robots, commonly used as sample changers, is sufficient to reliably position the plate, and to center and rotate the crystal as a goniometer would do on the beam axis – by combining the 6-axis degrees of freedom to emulate a single axis rotation distinct from the 6th rotation axis. The robot and beamline control software must also be adapted to enable these complex motions. The precision achieved upon rotation of a well-centered crystal is excellent, as shown by the small beam footprint left on a test crystal after a 60° rotation (figure 4D in Pinker and coworkers[49]). Three examples of this type of system are the commercial CATS,[50] ISARA and G-Rob[45] systems, in use at SLS, BESSY II, Soleil, Max IV and ESRF FIP (Table 1.1). A second approach is to use a dedicated, standard goniometer to move and to rotate the plate. The plate screening goniometer can simply be an adaptor on the main goniometer, or it can be distinct from the main goniometer for single crystal work, in which case fast goniometer switching procedures should be in place. The plate is either fixed manually to the goniometer with an adaptor holder in which the plate is placed or placed by an automatic sample changer. Recent examples (Figure 1.1) of such setups can be found at beamline I24[24,51] of the DLS, or the PLEX system at the Photon Factory.[31] The MD2 diffractometer can also take SBS plates using an adaptor (Table 1.1). SBS plate handling hardware has been developed for laboratory sources.[52] The Rigaku PlateMate system is one such example.

1.2.3 Plate Optimization for *In Situ*

The importance of the material composition and design of the plate for successful *in situ* data collection is fully appreciated.[6] Both the intensity and resolution of the scattering background must be minimized to increase the SNR. In particular, the background around the resolution limit should be minimized to maximize the SNR at the crystal's highest resolution. Amorphous materials are often preferred over crystalline or semi-crystalline materials due to their broader, more diffuse scattering properties.

The optical clarity, low birefringence and UV-compatibility, as well as the fabrication-related properties must also be considered. The intensity of the background generated by scattering from an amorphous material depends on several material- and geometry-related parameters:[53]

$$I_{bg} \propto A \frac{\rho V}{M_w} f_{bg}(s)^2 \tag{1.1}$$

where A is an absorption factor (which depends on the absorption coefficient μ_{abs} and thickness of the material), V is the illuminated volume (equal to the product of the beam area and the material thickness), ρ is the material mass density and M_w its molecular weight, and f_{bg} is the scattering-angle-dependent structure factor of the material. The proportionality factor, not shown in eqn (1.1), contains factors related to the detector pixel geometry and position, the X-ray beam characteristics, exposure time and physical constants. Upon inspection, eqn (1.1) shows that the background can be reduced by decreasing the material thickness, and selecting materials with suitable absorption and scattering properties, composed preferably of low-Z atoms.

Jacquamet and coworkers[6] compared several of the materials available at the time of their work. They recognized the need for the design of special *in situ* plates, with optimized well geometry and plastic thickness. Such an optimized plate, the Greiner CrystalQuick X45 for sitting-drop experiments, was introduced formally in 2011. The selected material was cyclic olefin copolymer (COC), a specialty plastic with low birefringence properties. The thickness of the well bottom was reduced to 300 μm, and the well shape allowed collection over a total angular range up to 80°. Later a second *in situ* optimized SBS plate was introduced, the MiTeGen InSitu-1 plate,[54] where the drops are directly deposited on a flat COC film of thickness 100 μm. The plates can be used for sitting- or hanging-drop experiments and are compatible with deposition of multiple drops by ADE. It is important to note that water permeability is of concern when using such thin plastic films, meaning that the drops dry faster.[25] In the latest *in situ* plate brought to market, the CrystalDirect plate developed at the European Molecular Biology Laboratory (EMBL) and available from MiTeGen, the COC film thickness has been reduced to 25 μm. The CrystalDirect plate is designed to be compatible with the automated harvesting system of the same name. Here the excess mother liquor is aspirated through a small hole, a pin is glued onto the film, laser photoablation is used to cut the film around the crystals and the glued pin tip and this is followed by immediate flash-cooling.[1,55]

1.2.4 Automation and Pipeline Integration

Automation compatibility was at the heart of the first plate screening experiments in 2004.[6] Further developments logically followed. In 2011, the first integrated plate screening pipeline was established at the Swiss Light

Source (SLS) beamline X06DA-PXIII.[9] In this setup, in addition to a simple short-term plate hotel inside the hutch, the sample changer has direct access to the Formulatrix Rock Imager RI 1000 plate hotel located in the adjacent crystallization facility. A 4-axis robot shuttles the plates through the radiation safety wall between the crystallization facility and beamline hutch. Using this automated system, based on the online access of drop imaging results from the automated imager, users can perform targeted *in situ* diffraction-based screening of their crystallization plates placed in the incubator without any onsite intervention after the setup of the plate. This arrangement facilitates fast feedback on the diffraction quality of the crystals, eliminates the need for risky plate transport or shipping, and enables fully remote plate screening operation. In addition, the X06DA-PXIII setup allows fast (2 minute) exchange by the users between standard cryogenic data collection and *in situ* screening mode.

Following this lead, the VMXi beamline,[56] a microfocus beamline dedicated fully to *in situ* plate screening and data collection, has been constructed at DLS. Two Formulatrix Rock Imagers set at two different incubation temperatures are installed in the beamline hutch and are directly accessed by the plate changer robot, which is mounted on a large linear axis. A system for maintaining temperature control on the plate during data collection is also foreseen. This beamline is expected to operate on a fully automated basis, where users mark the positions of interest on the images from the Rock Imager.

1.3 Further Developments: Scale Reduction and Microfluidics

The SBS format had its origins in automated laboratory equipment for liquid handling. In parallel to SBS-format *in situ* developments, there have also been *in situ* developments that use non-SBS formats, better adapted to data collection with standard goniometers at synchrotrons. These setups are often designed for direct data collection rather than screening. The departure from the SBS format goes generally in the direction of a format size reduction, both in the overall footprint, better compatible with crowded sample environments at beamlines, and in the crystallization trial dimensions, as with microfluidic setups. We have here arbitrarily distinguished between small format multi-crystal holders for *in situ* experiments and more classical microfluidics setups.

1.3.1 Small Formats

The X-chip (MiTeGen[61]) developed by Kisselman *et al.*[57] is a small plastic chip with drop positions marked, where micro-batch under oil crystallization trials can be set up (Figure 1.2a,b). Each drop location is defined by concentric hydrophilic–hydrophobic patterned rings, which ensure

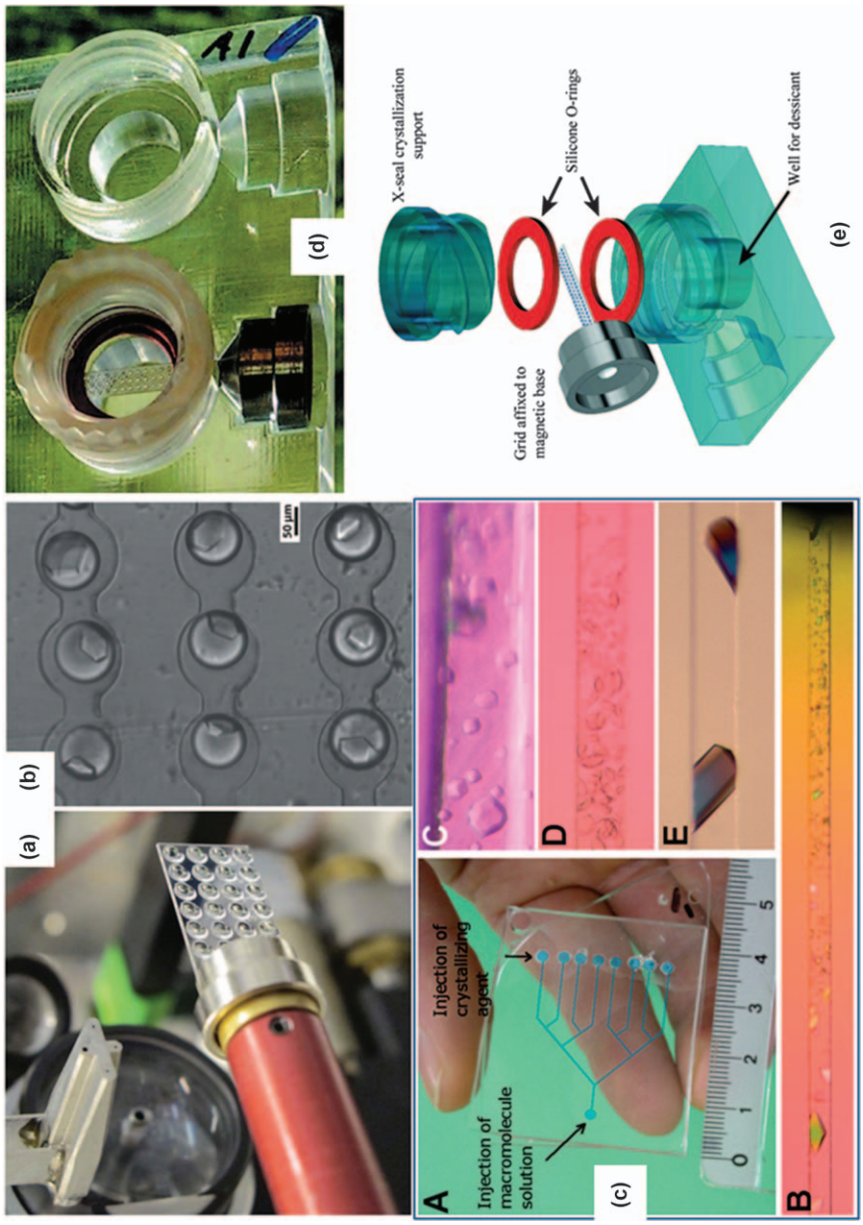

good pinning of the water-based crystallization drop and the oil cover layer. The crystallization drop is typically a 50 : 50 by volume mix of protein and precipitant solution (~500 nl total volume), covered with ~1 μl high viscosity oil (paraffin or a paraffin/silicon oil combination, typically). The drops will evaporate after days to weeks, depending on the oil. The chip itself absorbs about 30% of the beam (at 12.4 keV) with its 375 μm thickness and the oil contributing to the absorption and background. Nevertheless, Se-SAD phasing data collection was successfully demonstrated using this setup. To date, all data collection has been done at RT. The chip is fixed on a magnetic base compatible with standard goniometer heads, and the chip dimensions do not exceed this footprint, so that the X-chip is in principle compatible with any standard beamline setup.

More recently, Baxter *et al.*[60] introduced multi-crystal grids compatible with a home-developed tray for *in situ* crystal growth by vapor diffusion (Figure 1.2d,e). The grids consist of a laser-cut polycarbonate sheet of 100 to 200 μm thickness, with an array of holes, backed with a 5 μm polycarbonate foil. The holes are 125 to 400 μm in diameter. The grids are fixed on standard magnetic bases. In the *in situ* setup, the grid holes are filled with the protein solution and precipitant mixture, either with a liquid handling robot or by ADE. The grids are then installed in the vapor diffusion chamber, sealed with rubber O-rings and a removable lid. The chamber is opened after crystal growth. This type of multi-crystal mount is suitable for goniometer-based data collection both at synchrotrons and XFELs.[62]

ADE-assisted preparation of *in situ* samples has the potential for ligand or fragment screening experiments, as demonstrated by Yin and coworkers with *in situ* experiments set up on micromeshes.[63] Previously, Berger and coworkers[64] have shown that it is possible to grow crystals directly in a loop and to cryo-cool them.

1.3.2 Microfluidic Methods for *In Situ*

Microfluidics is the technique of choice for manipulating small volumes of liquids in a controlled manner. These *in situ* setups offer both the possibility to screen for various crystallization conditions and to collect diffraction data.

Figure 1.2 (a) X-CHIP with 24 wells mounted on a goniometer, reproduced under a Creative Commons License (https://creativecommons.org/licenses/by/2.0) from Kisselman *et al.*[57] Copyright © Kisselman *et al.* 2011. (b) Droplet-based microfluidic device for Laue diffraction on *in situ* grown glucose isomerase crystals, reproduced under a Creative Commons License (https://creativecommons.org/licenses/by/2.0) from Heymann *et al.*[58] Copyright © Michael Heymann *et al.* 2014. (c) On-chip counter diffusion chip (A), and channels with crystals of thaumatin (B), bovine insulin (C), a plant virus (D) and turkey egg-white lysozyme (E). Reproduced from Dhouib *et al.*[59] with permission from The Royal Society of Chemistry. (d, e) High density multi-crystal grids with *in situ* tray, reproduced under a Creative Commons License (https://creativecommons.org/licenses/by/2.0) from Baxter *et al.*[60]

Three types of on-chip crystallization experiments with *in situ* diffraction capabilities can be distinguished: free interface diffusion (FID), counter-diffusion and droplet-based batch. Most devices designed for on-chip data collection use COC as an X-ray-friendly material. However, new materials such as graphene have been tested and are of interest for their water-impermeability and ultralow-background properties.[65]

The main commercial option for FID microfluidics experiments is the Topaz chip in SBS format by Fluidigm,[66] which has been reported to be diffraction-compatible.[9] The Topaz system relies on the use of pressure-activated valves which bring into contact the preloaded precipitant and protein solutions, in up to 96 different conditions. FID experiments are characterized by small reaction chambers in which equilibration by diffusion is achieved relatively quickly and without convective mixing. As a result, the crystals produced by FID are potentially better ordered, and the trajectory in the crystallization phase diagram is better controlled compared to batch experiments.[67] Multilayer valve-based microfluidic devices optimized for *in situ* diffraction have also been reported,[68] with applications in Laue diffraction[69] and for *in meso* crystal growth.[70] Microfluidic FID experiments can screen conditions using small volumes, but the devices are usually difficult or expensive to fabricate and require a pump to operate.

Counter-diffusion differs from FID by the establishment of a gradient of conditions, by diffusion of chemical species over larger distances than in FID. In a single experiment a continuum of crystallization conditions is probed. Counter-diffusion in capillaries was among the first *in situ* diffraction setups,[4,5] and microfluidics soon appeared as a natural scale-down option, while offering more flexibility for channel design. Two groups, Ng and coworkers[71] and Dhouib and coworkers,[59] developed in parallel *in situ* counter-diffusion microfluidic chips. The device by Ng and coworkers[71] consists of single channels, and is commercialized by Greiner BioOne under the name CrystalSlide. Four CrystalSlides can be presented to the beam in a special SBS-format holder. In the commercial version, individual channels can be separated and mounted on a magnetic base.[72] The device by Dhouib and coworkers,[59] as well as the ChipX by Pinker and coworkers,[49] offers the possibility to screen different precipitant formulations against a single protein solution *via* channel branching (Figure 1.2c). The CrystalHarp system is an array of polyimide-coated quartz capillaries presented in SBS format,[9] commercialized by Molecular Dimensions.[73] Counter-diffusion devices are generally filled using pipettes, thus not requiring pump equipment.

Droplet-based microfluidics crystallization experiments are essentially microbatch-under-oil experiments. Each nanoliter trial droplet is separated from the others by a continuum of fluorocarbon oil. The droplets are produced by mixing two or more aqueous solutions, typically protein solution, buffer and precipitant, at the junction where the water-in-oil emulsion is created. The droplets are then stored on the device. Pumping equipment and careful flow or pressure control are required to create the droplets and to vary

the crystallization conditions. In the initial *in situ* droplet-based microfluidics measurements,[74] droplets were produced in devices made from PDMS, and stored for data collection in a 180 μm inner diameter glass capillary coupled to the device. For *in situ* data collection, the capillary containing the droplets was cut and sealed, and fixed on a magnetic base. The commercial CrystalCard device,[75,76] by Protein BioSolutions, works on the same principle. The crystals produced can be harvested or measured *in situ*, either directly inside the chip or by coupling with a capillary.[77] The Plug Maker system includes the pumping equipment and automated controls needed to use the CrystalCard devices. More recently, other X-ray-friendly chips for droplet-based *in situ* experiments have been designed by Heymann *et al.*,[58] using thin COC films for device fabrication. The suitability of the device for serial Laue diffraction data collection at RT was demonstrated. The effects of a confined droplet environment on nucleation and crystallization processes were studied in detail.[78] It was found that a preliminary screening step makes it possible to find conditions where only a single crystal per droplet is obtained, which is an optimal situation for data collection. This was attributed to a confinement-induced negative feedback on the nucleation probability after the first nucleus appeared.

1.4 The Emergence of Serial *In Situ* Data Collection

1.4.1 Thin-film Sandwiches

In recent years, a new class of *in situ* setups has been developed, that we will refer to here as thin-film sandwiches to distinguish them from the previously described *in situ* setups. The motivation for these new developments is to offer a user-friendly setup that can be prepared with standard crystallization equipment and that is compatible with *in situ* serial crystallography. The principle of thin-film sandwich setups is to perform the crystallization trial in a confined space between two thin, X-ray compatible films. To avoid dehydration caused by water permeability of the film, the sandwich is enclosed in a second thick glass or plastic sandwich for the duration of the crystallization experiment and this is removed just before data collection (Figure 1.3). These methods are appropriately called double-sandwich methods. The thin-film sandwich plate has an SBS 96-well plate format that is compatible with laboratory drop setting robotics. In contrast to SBS *in situ* plates (Section 1.2), individual wells can be easily removed from the plate. This allows for direct mounting of wells on standard goniometers. Importantly, individual wells can be flash-cooled in liquid nitrogen, which extends *in situ* crystallography from mainly a screening technique at RT to a routine data collection method at cryogenic temperature. The wells can be fixed on standard pins, flash-cooled, shipped in a dry-shipper and mounted on a goniometer with an automated sample changer as commonly practiced in single crystal cryo-crystallography. Therefore, beam interrogation on *in situ* thin-film sandwiches can be performed either at RT[11] or under cryogenic

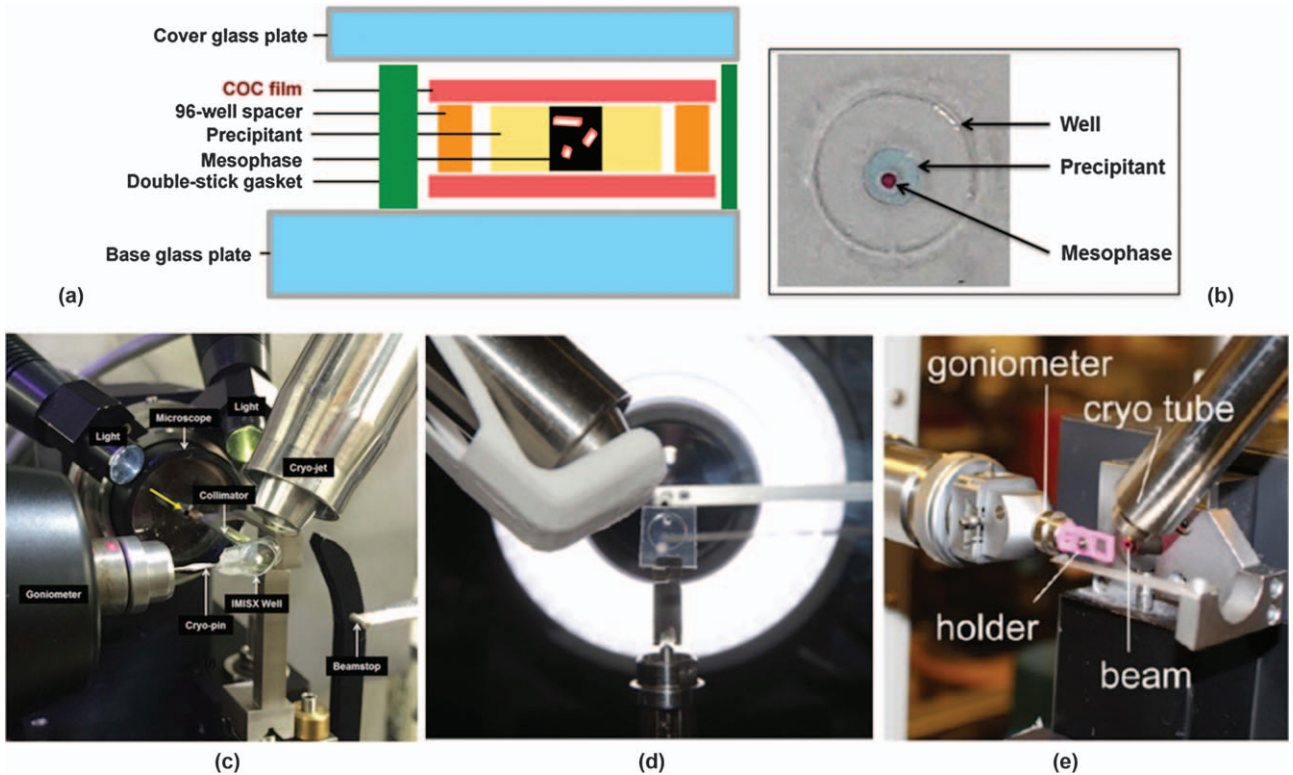

Figure 1.3 Schematic (a) and picture (b) of a well of the IMISX plate, reproduced under a Creative Commons License (https://creativecommons.org/licenses/by/2.0) from Huang *et al.*[11] (c) Cryo-cooled COC IMISX well at the X06SA-PXI beamline at the SLS, reproduced under a Creative Commons License (https://creativecommons.org/licenses/by/2.0) from Huang *et al.*[32] (d) Room temperature COP double sandwich setup at DLS I24, reproduced under a Creative Commons License (https://creativecommons.org/licenses/by/2.0) from Axford *et al.*[79] (e) Mylar double sandwich setup at the APS GM/*CA* beamlines, reproduced from ref. 28 (http://pubs.acs.org/doi/abs/10.1021/acs.cgd.6b00950), with permission from the American Chemical Society.[28]

conditions.[32] The flat geometry also offers a potentially larger data collection angular range compared to SBS *in situ* plates with curved wells, which is particularly attractive for application in the emerging serial crystallography field. Clearly-explained procedures for plate setup and easy-to-handle commercial solutions are now available,[11,32] providing thin-film sandwich methods with opportunities for rapid expansion and wide-spread use.

Careful selection of the thin film material is necessary to minimize the absorption and diffraction background contribution. A material with negligible absorption and background scattering would be ideal. However, in practice, it is sufficient if the absorption and background scattering of the thin film is low in comparison to the contribution from the crystallization medium. In addition, particular care must be taken to minimize the background scattering near the diffraction resolution limit of the crystals, where the diffraction signals are weak. This is usually around 2.5–4 Å for most targets. Plastic films are often used for their low cost, easy handling and the commercial availability of films with relatively low thicknesses. Nonetheless, they can have ring-featured background[28] and their water-tightness is often relatively low. Reported film variants include 25 μm COC,[11] 13 μm cyclic olefin polymer (COP),[79] 8 μm Kapton[80] and 3.5 μm Mylar.[28] The currently available commercial setups use 25 μm COC (IMISX™ by MiTeGen[81]) and 40 μm plastic film (DiffraX™ by Molecular Dimensions[82]). Other materials such as silicon nitride membranes, with sub-micrometer to nanometer thicknesses and low water permeability, have also been used. However, these are fragile, difficult to handle, are more expensive,[83] and are used mainly for data collection purposes. The thickness of the spacer between the two thin films in the sandwich defines sample thickness. The spacer thickness is therefore a major parameter in the optimization of background. The spacer thicknesses reported in the literature range from 50 to 140 μm. Commercial setups come with 140 μm (IMISX™ by MiTeGen[81]) and 100 μm (DiffraX™ by Molecular Dimensions[82]) spacers. In the DiffraX™ setup by Molecular Dimensions, the spacer is already fixed on the base film for ease of handling. Thinner spacers are commercially available. However, issues of preferential orientation of crystals, influence on the crystallization conditions and difficulty of handling have been reported with thinner spacers.[28] Figure 1.4 shows representative background curves corresponding to the contribution of each of the components of the thin-film sandwich in the current IMISX™ setup by MiTeGen. The COC film has maximum scatter at intermediate resolution (4–6 Å), while at higher scattering angles the matrix (LCP and precipitant solution) gives the most significant contribution because of the spacer thickness. Thin silicon nitride has virtually zero background, which becomes beneficial compared to plastic films in cases where the spacer used is relatively thin. Dedicated holders for securing the sample on standard magnetic goniometers have been developed by several groups[28,79] and some are commercially available.

Thin-film methods were developed originally for *in meso* or LCP crystallization, since the high viscosity of the mesophase in which crystallization takes place makes it difficult to harvest crystals, and the method often yields

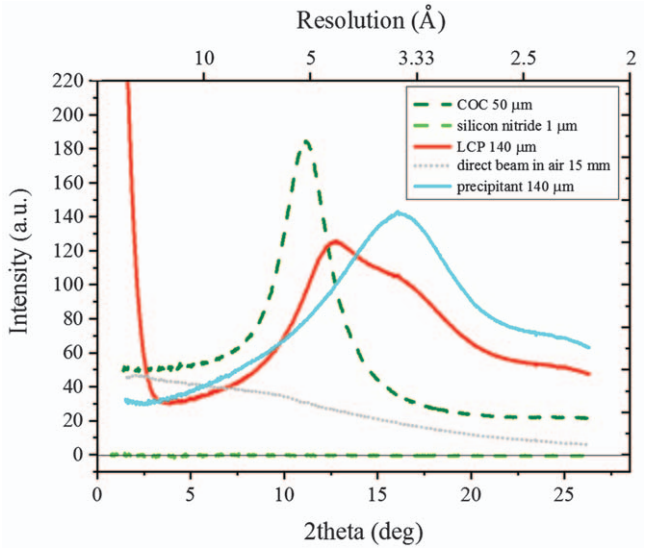

Figure 1.4 Representative background contribution curves from the different components of a typical IMISX plate: 2×25 µm COC, 140 µm LCP or precipitant matrix (from the spacer thickness). The contribution curves were obtained by deconvolution from total background data taken at various points of the well. For comparison, the contribution of 1 µm silicon nitride is also shown, as well as the scattering from 15 mm of direct beam path in air (obtained by subtraction from images taken with two different beamstop distances). The data was measured at beamline X06SA-PXI of the SLS, at 12.67 keV, 1 s exposure with flux of 4×10^{11} ph s^{-1}, beam size 20 µm×10 µm, detector distance 400 mm, and beamstop distances 10 and 25 mm.

small crystals. The sandwich film, of controlled thickness and flat geometry, provides a conveniently rigid scaffold with which to handle the sample, and to clearly view the crystals just as with standard glass LCP plates. On the other hand, thanks to the mesophase viscosity, handling of the samples is possible without perturbing the crystal growth environment. It has been demonstrated that thin-film sandwich setups are compatible with crystallization and data collection for water soluble proteins as well, with and without a mesophase growth medium.[28,79]

Data collection and screening are typically performed in the same way in thin-film sandwich setups. Small wedges of data are collected on a large number of micro-crystals in serial fashion at a microfocus beamline. This mode of data collection is very well suited for full automation in combination with rastering. Examples of such automated serial collection utilities include the MeshAndCollect system[39] at the ESRF, the Zoo system[84] at SPring-8 and the CY+ system at SLS (unpublished).

Thin-film sandwich setups have been demonstrated by Huang *et al.*[11,32] to be compatible with data collection for experimental phasing. This includes

bromine and native SAD phasing of various proteins. Key to the success of the process was the accumulation of enough data to extract weak anomalous signals. Schubert *et al.*[80] have explored the suitability of the setup for time-resolved dynamic studies at RT, using a dose-dependent study of the progress of radiation damage on a model protein as an example. The number of crystals required for a complete data set depends on the conditions (RT or cryo), crystal size, space group and phasing method. For example, in the work of Huang *et al.*, in the case of lysozyme at RT,[11] about 100 crystals of around 20 μm in size from 2 wells were needed to solve the structure by molecular replacement, 200 crystals from 4 wells were needed for bromide single wavelength anomalous diffraction (SAD) phasing, while 1000 crystals of from 12 wells were needed for native SAD phasing. Under cryogenic conditions,[32] only a handful of crystals were needed in similar circumstances. For instance, only six 30 μm crystals were required to solve an insulin structure by native SAD. For membrane proteins, significantly more crystals are generally required due to their smaller size, weaker diffraction and enhanced radiation sensitivity. Typically, with a microfocused beam, a few images per crystal can be obtained at RT, and a partial data set under cryogenic conditions, depending on the radiation damage threshold.

1.4.2 Liquid Manipulation Methods

The liquid manipulation methods briefly covered in this section might be considered *in situ* by the absence of manual crystal handing. Post-crystal growth, ADE methods are an emerging sample delivery scheme. They come with a few variants, but all involve the use of acoustic waves of defined frequency propagating through a liquid suspension to deform the surface so as to create droplets of controllable size. Crystals can be trapped in the droplets, which are either presented directly to the beam, ideally in a drop-on-demand fashion,[85] or are deposited on a conveyor belt or tape drive.[86,87,98] Another variant involves trapping the drop in an acoustic standing wave field.[88] However, acoustic droplet manipulation can be difficult in the presence of surfactants, as it is often the case for crystallization of membrane proteins in solution.

Inherited from XFEL sample delivery techniques, injection methods can be compared to *in situ* methods, at least when the crystals are not filtered, pressurized or transferred to or mixed with a different matrix after crystal growth.[89] This corresponds to cases of microcrystals grown in liquid by batch methods and directly injected in a capillary[90] or in a microfluidic trap.[91] Electrospinning injection[92,93] is another liquid delivery technique where mixing is not required. Crystals grown in LCP can also be injected sufficiently slowly for synchrotron serial data collection[30,94,95] using a high-viscosity injector. Injection delivery methods have been covered by several previous reviews,[96] to which the interested reader is referred. Manipulation of microcrystals often involves pipetting, which can be considered as relatively mild handling compared to standard harvesting.[97]

1.5 Conclusion and Outlook

In this chapter we have covered the wide variety of *in situ* crystal growth and diffraction setups available, including SBS-format plates, microfluidics, and thin-film sandwich methods. *In situ* method development is a dynamic field, where new approaches, materials and equipment are being introduced by user groups and facilities on a regular basis. All the methods covered here will continue to benefit from progress in materials manufacturing, for further optimization of thickness and background properties of plates and films.

The development of synchrotron sources will give access to increasingly higher flux densities with the emergence of diffraction limited storage rings at 4th generation synchrotrons. These include the new MAX IV facility in Sweden and the planned upgrades at many 3rd generation sources. The low emittance of this new type of facility naturally increases the flux density and makes it easier to obtain stable microfocused beams useful for *in situ* data collection. Also on the horizon are 'pink beam' beamlines. These provide bandwidths of the order of 0.1–1% *via* multilayer monochromator, in contrast to silicon (111) crystal monochromators with a bandwidth of ~0.02%. The wider bandwidth results in an increase of flux density but also broadens reflections and increases scattering background, which might lower the SNR of weak reflections and create problems due to reflection overlap when used with large unit cell crystals.

Future developments in *in situ* data collection will aim to optimize SNR for smaller crystals and to improve experimental phasing possibilities, in particular for thin-film sandwich setups. *In situ* experimental phasing using heavy atom derivatives and native lighter anomalous scatterers (sulfur, phosphorous, calcium, *etc.*) has already been demonstrated. However, measurement of very small anomalous differences still requires large amounts of data and careful optimization of the SNR, and radiation damage remains an issue. Improvements in crystallization setups and materials, beamline automation and data processing will contribute to making serial experimental phasing a more routine data collection method. One of the next avenues to explore will be the use of serial *in situ* data collection for ligand screening and fragment based drug design. This type of high-throughput application will require improved automation of data collection and data processing. Finally, serial *in situ* techniques call for specific user training to make the new techniques available to all. Towards this end, detailed protocols have been published, including instructional videos,[11,32] and training workshops take place regularly in different facilities.

Acknowledgements

We acknowledge Laura Vera, May Marsh and Chia-Ying Huang for stimulating discussions.

References

1. U. Zander, G. Hoffmann, I. Cornaciu, J.-P. Marquette, G. Papp, C. Landret, G. Seroul, J. Sinoir, M. Röwer, F. Felisaz, S. Rodriguez-Puente, V. Mariaule, P. Murphy, M. Mathieu, F. Cipriani and J. A. Márquez, *Acta Crystallogr., Sect. D: Struct. Biol.*, 2016, **72**, 454–466.
2. P. Roedig, I. Vartiainen, R. Duman, S. Panneerselvam, N. Stübe, O. Lorbeer, M. Warmer, G. Sutton, D. I. Stuart, E. Weckert, C. David, A. Wagner and A. Meents, *Sci. Rep.*, 2015, **5**, 10451.
3. C. Mueller, A. Marx, S. W. Epp, Y. Zhong, A. Kuo, A. R. Balo, J. Soman, F. Schotte, H. T. Lemke, R. L. Owen, E. F. Pai, A. R. Pearson, J. S. Olson, P. A. Anfinrud, O. P. Ernst and R. J. Dwayne Miller, *Struct. Dyn.*, 2015, **2**, 054302.
4. J. M. Garciaruiz, A. Moreno, C. Viedma and M. Coll, *Mater. Res. Bull.*, 1993, **28**, 541–546.
5. F. J. López-Jaramillo, J. M. García-Ruiz, J. A. Gavira and F. Otálora, *J. Appl. Crystallogr.*, 2001, **34**, 365–370.
6. L. Jacquamet, J. Ohana, J. Joly, F. Borel, M. Pirocchi, P. Charrault, A. Bertoni, P. Israel-Gouy, P. Carpentier, F. Kozielski, D. Blot and J.-L. Ferrer, *Structure*, 2004, **12**, 1219–1225.
7. C. Porta, A. Kotecha, A. Burman, T. Jackson, J. Ren, S. Loureiro, I. M. Jones, E. E. Fry, D. I. Stuart and B. Charleston, *PLoS Pathog.*, 2013, **9**, e1003255.
8. J. A. Newman, S. Zhang, S. Z. Sullivan, X. Y. Dow, M. Becker, M. J. Sheedlo, S. Stepanov, M. S. Carlsen, R. M. Everly, C. Das, R. F. Fischetti and G. J. Simpson, *J. Synchrotron Radiat.*, 2016, **23**, 959–965.
9. R. Bingel-Erlenmeyer, V. Olieric, J. P. A. Grimshaw, J. Gabadinho, X. Wang, S. G. Ebner, A. Isenegger, R. Schneider, J. Schneider, W. Glettig, C. Pradervand, E. H. Panepucci, T. Tomizaki, M. Wang and C. Schulze-Briese, *Cryst. Growth Des.*, 2011, **11**, 916–923.
10. M. Gelin, V. Delfosse, F. Allemand, F. Hoh, Y. Sallaz-Damaz, M. Pirocchi, W. Bourguet, J. L. Ferrer, G. Labesse and J. F. C. C. Guichou, *Acta Crystallogr., Sect. D: Biol. Crystallogr.*, 2015, **71**, 1777–1787.
11. C. Y. Huang, V. Olieric, P. Ma, E. Panepucci, K. Diederichs, M. Wang and M. Caffrey, *Acta Crystallogr., Sect. D: Biol. Crystallogr.*, 2015, **71**, 1238–1256.
12. J. L. Smith, R. F. Fischetti and M. Yamamoto, *Curr. Opin. Struct. Biol.*, 2012, **22**, 602–612.
13. K. Diederichs and M. Wang, in *Protein Crystallography: Methods and Protocols*, 2017, ch. 10.
14. I. Schlichting, *IUCrJ*, 2015, **2**, 246–255.
15. J. M. Martin-Garcia, C. E. Conrad, J. Coe, S. Roy-Chowdhury and P. Fromme, *Arch. Biochem. Biophys.*, 2016, **602**, 32–47.
16. C. Abergel, *Acta Crystallogr., Sect. D: Biol. Crystallogr.*, 2004, **60**, 1413–1416.
17. A. Douangamath, P. Aller, P. Lukacik, J. Sanchez-Weatherby, I. Moraes and J. Brandao-Neto, *Acta Crystallogr., Sect. D: Biol. Crystallogr.*, 2013, **69**, 920–923.

18. E. F. Garman, *Acta Crystallogr., Sect. D: Biol. Crystallogr.*, 2010, **66**, 339–351.
19. R. J. Southworth-Davies, M. A. Medina, I. Carmichael and E. F. Garman, *Structure*, 2007, **15**, 1531–1541.
20. R. Henderson, *Proc. R. Soc. B*, 1990, **241**, 6–8.
21. R. L. Owen, E. Rudino-Pinera and E. F. Garman, *Proc. Natl. Acad. Sci. U. S. A.*, 2006, **103**, 4912–4917.
22. T. Weinert, V. Olieric, S. Waltersperger, E. Panepucci, L. Chen, H. Zhang, D. Zhou, J. Rose, A. Ebihara, S. Kuramitsu, D. Li, N. Howe, G. Schnapp, A. Pautsch, K. Bargsten, A. E. Prota, P. Surana, J. Kottur, D. T. Nair, F. Basilico, V. Cecatiello, S. Pasqualato, A. Boland, O. Weichenrieder, B. C. Wang, M. O. Steinmetz, M. Caffrey and M. Wang, *Nat. Methods*, 2015, **12**, 131–133.
23. J. M. Holton, *J. Synchrotron Radiat.*, 2009, **16**, 133–142.
24. D. Axford, R. L. Owen, J. Aishima, J. Foadi, A. W. Morgan, J. I. Robinson, J. E. Nettleship, R. J. Owens, I. Moraes, E. E. Fry, J. M. Grimes, K. Harlos, A. Kotecha, J. S. Ren, G. Sutton, T. S. Walter, D. I. Stuart and G. Evans, *Acta Crystallogr., Sect. D: Struct. Biol.*, 2012, **68**, 592–600.
25. L. E. Zipper, X. Aristide, D. P. Bishop, I. Joshi, J. Kharzeev, K. B. Patel, B. M. Santiago, K. Joshi, K. Dorsinvil, R. M. Sweet and A. S. Soares, *Acta Crystallogr., Sect. F: Struct. Biol. Commun.*, 2014, **70**, 1707–1713.
26. V. Cherezov and M. Caffrey, *J. Appl. Crystallogr.*, 2006, **39**, 604–606.
27. K. Michalska, K. Tan, C. Chang, H. Li, C. Hatzos-Skintges, M. Molitsky, R. Alkire and A. Joachimiak, *J. Synchrotron Radiat.*, 2015, **22**, 1386–1395.
28. J. Broecker, V. Klingel, W.-L. Ou, A. R. Balo, D. J. Kissick, C. M. Ogata, A. Kuo and O. P. Ernst, *Cryst. Growth Des.*, 2016, **16**, 6318–6326.
29. U. Mueller, N. Darowski, M. R. Fuchs, R. Forster, M. Hellmig, K. S. Paithankar, S. Puhringer, M. Steffien, G. Zocher and M. S. Weiss, *J. Synchrotron Radiat.*, 2012, **19**, 442–449.
30. P. Nogly, D. James, D. Wang, T. A. White, N. Zatsepin, A. Shilova, G. Nelson, H. Liu, L. Johansson, M. Heymann, K. Jaeger, M. Metz, C. Wickstrand, W. Wu, P. Båth, P. Berntsen, D. Oberthuer, V. Panneels, V. Cherezov, H. N. Chapman, G. Schertler, R. Neutze, J. Spence, I. Moraes, M. Burghammer, J. Standfuss and U. Weierstall, *IUCrJ*, 2015, **2**, 1–9.
31. Y. Yamada, M. Hiraki, N. Matsugaki, R. Kato and T. Senda, Proceedings of the 12th International Conference on Synchrotron Radiation Instrumentation – SRI2015, New York, USA, 2015.
32. C.-Y. Huang, V. Olieric, P. Ma, N. Howe, L. Vogeley, X. Liu, R. Warshamanage, T. Weinert, E. Panepucci, B. Kobilka, K. Diederichs, M. Wang and M. Caffrey, *Acta Crystallogr., Sect. D: Struct. Biol.*, 2016, **72**, 93–112.
33. K. Hirata, Y. Kawano, G. Ueno, K. Hashimoto, H. Murakami, K. Hasegawa, T. Hikima, T. Kumasaka and M. Yamamoto, *J. Phys.: Conf. Ser.*, 2013, **425**, 012002.

34. J. A. Wojdyla, E. Panepucci, I. Martiel, S. Ebner, C.-Y. Huang, M. Caffrey, O. Bunk and M. Wang, *J. Appl. Crystallogr.*, 2016, **49**, 944–952.
35. L. Jacquamet, J. Ohana, J. Joly, P. Legrand, R. Kahn, F. Borel, M. Pirocchi, P. Charrault, P. Carpentier and J. L. Ferrer, *Acta Crystallogr., Sect. D: Biol. Crystallogr.*, 2004, **60**, 888–894.
36. M. Roth, P. Carpentier, O. Kaïkati, J. Joly, P. Charrault, M. Pirocchi, R. Kahn, E. Fanchon, L. Jacquamet, F. Borel, A. Bertoni, P. Israel-Gouy and J.-L. Ferrer, *Acta Crystallogr., Sect. D: Biol. Crystallogr.*, 2002, **58**, 805–814.
37. D. Nurizzo, M. W. Bowler, H. Caserotto, F. Dobias, T. Giraud, J. Surr, N. Guichard, G. Papp, M. Guijarro, C. Mueller-Dieckmann, D. Flot, S. McSweeney, F. Cipriani, P. Theveneau and G. A. Leonard, *Acta Crystallogr., Sect. D: Struct. Biol.*, 2016, **72**, 966–975.
38. V. Cherezov, M. A. Hanson, M. T. Griffith, M. C. Hilgart, R. Sanishvili, V. Nagarajan, S. Stepanov, R. F. Fischetti, P. Kuhn and R. C. Stevens, *J. R .Soc., Interface*, 2009, **6**(Suppl 5), S587–S597.
39. U. Zander, G. Bourenkov, A. N. Popov, D. de Sanctis, O. Svensson, A. A. McCarthy, E. Round, V. Gordeliy, C. Mueller-Dieckmann and G. A. Leonard, *Acta Crystallogr., Sect. D: Biol. Crystallogr.*, 2015, **71**, 2328–2343.
40. G. Assmann, W. Brehm and K. Diederichs, *J. Appl. Crystallogr.*, 2016, **49**, 1021–1028.
41. R. Giordano, R. M. Leal, G. P. Bourenkov, S. McSweeney and A. N. Popov, *Acta Crystallogr., Sect. D: Biol. Crystallogr.*, 2012, **68**, 649–658.
42. J. Foadi, P. Aller, Y. Alguel, A. Cameron, D. Axford, R. L. Owen, W. Armour, D. G. Waterman, S. Iwata and G. Evans, *Acta Crystallogr., Sect. D: Biol. Crystallogr.*, 2013, **69**, 1617–1632.
43. P. Aller, J. Sanchez-Weatherby, J. Foadi, G. Winter, C. M. C. Lobley, D. Axford, A. W. Ashton, D. Bellini, J. Brandao-Neto, S. Culurgioni, A. Douangamath, R. Duman, G. Evans, S. Fisher, R. Flaig, D. R. Hall, P. Lukacik, M. Mazzorana, K. E. McAuley, V. Mykhaylyk, R. L. Owen, N. G. Paterson, P. Romano, J. Sandy, T. Sorensen, F. von Delft, A. Wagner, A. Warren, M. Williams, D. I. Stuart and M. A. Walsh, *Methods Mol. Biol.*, 2015, **1261**, 233–253.
44. A. E. Bruno, A. S. Soares, R. L. Owen and E. H. Snell, *J. Appl. Crystallogr.*, 2016, **49**, 2082–2090.
45. A. le Maire, M. Gelin, S. Pochet, F. Hoh, M. Pirocchi, J. F. Guichou, J. L. Ferrer and G. Labesse, *Acta Crystallogr., Sect. D: Biol. Crystallogr.*, 2011, **67**, 747–755.
46. D. Axford, J. Foadi, N.-J. Hu, H. G. Choudhury, S. Iwata, K. Beis, G. Evans and Y. Alguel, *Acta Crystallogr., Sect. D: Biol. Crystallogr.*, 2015, **71**, 1228–1237.
47. A. Burkhardt, A. Wagner, M. Warmer, R. Reimer, H. Hohenberg, J. Ren, E. E. Fry, D. I. Stuart and A. Meents, *Acta Crystallogr., Sect. D: Biol. Crystallogr.*, 2013, **69**, 308–312.

48. E. Teplitsky, K. Joshi, D. L. Ericson, A. Scalia, J. D. Mullen, R. M. Sweet and A. S. Soares, *J. Struct. Biol.*, 2015, **191**, 49–58.
49. F. Pinker, M. Brun, P. Morin, A.-L. Deman, J.-F. Chateaux, V. Oliéric, C. Stirnimann, B. Lorber, N. Terrier, R. Ferrigno and C. Sauter, *Cryst. Growth Des.*, 2013, **13**, 3333–3340.
50. L. Jacquamet, J. Joly, A. Bertoni, P. Charrault, M. Pirocchi, X. Vernede, F. Bouis, F. Borel, J. P. Périn, T. Denis, J. L. Rechatin and J. L. Ferrer, *J. Synchrotron Radiat.*, 2009, **16**, 14–21.
51. V. Grama, D. Axford, G. Duller, M. Burt and R. L. Owen, I24 Endstation upgrade - overview and engineering design, MEDSI 2014 Conference Melbourne, Australia, 2014.
52. D. Hargreaves, *J. Appl. Crystallogr.*, 2012, **45**, 138–140.
53. J. M. Holton, S. Classen, K. A. Frankel and J. A. Tainer, *FEBS J.*, 2014, **281**, 4046–4060.
54. MiTeGen, In-Situ-01™Crystallization Plate, http://www.mitegen.com/products/plates/insitu1/brochure.pdf (accessed on 03.02.2017).
55. F. Cipriani, M. Röwer, C. Landret, U. Zander, F. Felisaz and J. A. Márquez, *Acta Crystallogr., Sect. D: Biol. Crystallogr.*, 2012, **68**, 1393–1399.
56. VMXi beamline at Diamond Light Source, http://www.diamond.ac.uk/Beamlines/Mx/VMXi.html (accessed on 19.02.2017).
57. G. Kisselman, W. Qiu, V. Romanov, C. M. Thompson, R. Lam, K. P. Battaile, E. F. Pai and N. Y. Chirgadze, *Acta Crystallogr., Sect. D: Biol. Crystallogr.*, 2011, **67**, 533–539.
58. M. Heymann, A. Opathalage, J. L. Wierman, S. Akella, D. M. E. Szebenyi, S. M. Gruner and S. Fraden, *IUCrJ*, 2014, **1**, 349–360.
59. K. Dhouib, C. Khan Malek, W. Pfleging, B. Gauthier-Manuel, R. Duffait, G. Thuillier, R. Ferrigno, L. Jacquamet, J. Ohana, J.-L. Ferrer, A. Théobald-Dietrich, R. Giegé, B. Lorber and C. Sauter, *Lab Chip*, 2009, **9**, 1412–1421.
60. E. L. Baxter, L. Aguila, R. Alonso-Mori, C. O. Barnes, C. A. Bonagura, W. Brehmer, A. T. Brunger, G. Calero, T. T. Caradoc-Davies, R. Chatterjee, W. F. Degrado, J. S. Fraser, M. Ibrahim, J. Kern, B. K. Kobilka, A. C. Kruse, K. M. Larsson, H. T. Lemke, A. Y. Lyubimov, A. Manglik, S. E. McPhillips, E. Norgren, S. S. Pang, S. M. Soltis, J. Song, J. Thomaston, Y. Tsai, W. I. Weis, R. A. Woldeyes, V. Yachandra, J. Yano, A. Zouni and A. E. Cohen, *Acta Crystallogr., Sect. D: Struct. Biol.*, 2016, **72**, 1–10.
61. XChip information, http://www.mitegen.com/product/x-chip/ (accessed on 18.03.2018).
62. A. E. Cohen, S. M. Soltis, A. Gonzalez, L. Aguila, R. Alonso-Mori, C. O. Barnes, E. L. Baxter, W. Brehmer, A. S. Brewster, A. T. Brunger, G. Calero, J. F. Chang, M. Chollet, P. Ehrensberger, T. L. Eriksson, Y. Feng, J. Hattne, B. Hedman, M. Hollenbeck, J. M. Holton, S. Keable, B. K. Kobilka, E. G. Kovaleva, A. C. Kruse, H. T. Lemke, G. Lin, A. Y. Lyubimov, A. Manglik, Mathews II, S. E. McPhillips, S. Nelson, J. W. Peters, N. K. Sauter, C. A. Smith, J. Song, H. P. Stevenson, Y. Tsai, M. Uervirojnangkoorn, V. Vinetsky, S. Wakatsuki, W. I. Weis,

O. A. Zadvornyy, O. B. Zeldin, D. Zhu and K. O. Hodgson, *Proc. Natl. Acad. Sci. U. S. A.*, 2014, **111**, 17122–17127.
63. X. Yin, A. Scalia, L. Leroy, C. M. Cuttitta, G. M. Polizzo, D. L. Ericson, C. G. Roessler, O. Campos, M. Y. Ma, R. Agarwal, R. Jackimowicz, M. Allaire, A. M. Orville, R. M. Sweet and A. S. Soares, *Acta Crystallogr., Sect. D: Biol. Crystallogr.*, 2014, **70**, 1177–1189.
64. M. A. Berger, J. H. Decker and Mathews II, *J. Appl. Crystallogr.*, 2010, **43**, 1513–1518.
65. S. Sui, Y. Wang, K. W. Kolewe, V. Srajer, R. Henning, J. D. Schiffman, C. Dimitrakopoulos and S. L. Perry, *Lab Chip*, 2016, **16**, 3082–3096.
66. J. E. Lee, M. L. Fusco and E. O. Saphire, *Nat. Protoc.*, 2009, **4**, 592–604.
67. I. Russo Krauss, A. Merlino, A. Vergara and F. Sica, *Int. J. Mol. Sci.*, 2013, **14**, 11643–11691.
68. S. Guha, S. L. Perry, A. S. Pawate and P. J. Kenis, *Sens. Actuators, B*, 2012, **174**, 1–9.
69. S. L. Perry, S. Guha, A. S. Pawate, R. Henning, I. Kosheleva, V. Srajer, P. J. Kenis and Z. Ren, *J. Appl. Crystallogr.*, 2014, **47**, 1975–1982.
70. D. S. Khvostichenko, J. M. Schieferstein, A. S. Pawate, P. D. Laible and P. J. A. Kenis, *Cryst. Growth Des.*, 2014, **14**, 4886–4890.
71. J. D. Ng, P. J. Clark, R. C. Stevens and P. Kuhn, *Acta Crystallogr., Sect. D: Biol. Crystallogr.*, 2008, **64**, 189–197.
72. CrystalSlide information, http://www.mitegen.com/products/plates/CrystalSlide_UserGuide_E.pdf (accessed on 16.02.2017).
73. CrystalHarp information, https://www.moleculardimensions.com/applications/upload/Crystalharp%20flyer_UK.pdf (accessed on 16.02.2017).
74. B. Zheng, J. D. Tice, L. S. Roach and R. F. Ismagilov, *Angew. Chem., Int. Ed. Engl.*, 2004, **43**, 2508–2511.
75. C. J. Gerdts, M. Elliott, S. Lovell, M. B. Mixon, A. J. Napuli, B. L. Staker, P. Nollert and L. Stewart, *Acta Crystallogr., Sect. D: Biol. Crystallogr.*, 2008, **64**, 1116–1122.
76. J. Christensen, C. J. Gerdts, M. C. Clifton and L. Stewart, *Acta Crystallogr., Sect. F: Struct. Biol. Cryst. Commun.*, 2011, **67**, 1022–1026.
77. M. K. Yadav, C. J. Gerdts, R. Sanishvili, W. W. Smith, L. S. Roach, R. F. Ismagilov, P. Kuhn and R. C. Stevens, *J. Appl. Crystallogr.*, 2005, **38**, 900–905.
78. S. V. Akella, A. Mowitz, M. Heymann and S. Fraden, *Cryst. Growth Des.*, 2014, **14**, 4487–4509.
79. D. Axford, P. Aller, J. Sanchez-Weatherby and J. Sandy, *Acta Crystallogr., Sect. F: Struct. Biol. Cryst. Commun.*, 2016, **72**, 313–319.
80. R. Schubert, S. Kapis, Y. Gicquel, G. Bourenkov, T. R. Schneider, M. Heymann, C. Betzel and M. Perbandt, *IUCrJ*, 2016, **3**, 393–401.
81. MiTeGen webpage, http://www.mitegen.com/lcp/imisx/ (accessed on 17.02.2017).
82. A. Savill, personal communication.
83. V. Cherezov and M. Caffrey, *Faraday Discuss.*, 2007, **136**, 195.

84. K. Hirata, Towards Automatic Data Collection Pipeline for Membrane Protein Structure Analyses at Beamline BL32XU, Synchrotron Radiation and Instrumentation 2015 conference, 2015.
85. C. G. Roessler, R. Agarwal, M. Allaire, R. Alonso-Mori, B. Andi, J. F. R. Bachega, M. Bommer, A. S. Brewster, M. C. Browne, R. Chatterjee, E. Cho, A. E. Cohen, M. Cowan, S. Datwani, V. L. Davidson, J. Defever, B. Eaton, R. Ellson, Y. Feng, L. P. Ghislain, J. M. Glownia, G. Han, J. Hattne, J. Hellmich, A. Héroux, M. Ibrahim, J. Kern, A. Kuczewski, H. T. Lemke, P. Liu, L. Majlof, W. M. McClintock, S. Myers, S. Nelsen, J. Olechno, A. M. Orville, N. K. Sauter, A. S. Soares, S. M. Soltis, H. Song, R. G. Stearns, R. Tran, Y. Tsai, M. Uervirojnangkoorn, C. M. Wilmot, V. Yachandra, J. Yano, E. T. Yukl, D. Zhu and A. Zouni, *Structure*, 2016, 631–640.
86. C. G. Roessler, A. Kuczewski, R. Stearns, R. Ellson, J. Olechno, A. M. Orville, M. Allaire, A. S. Soares and A. Héroux, *J. Synchrotron Radiat.*, 2013, **20**, 805–808.
87. F. D. Fuller, S. Gul, R. Chatterjee, E. S. Burgie, I. D. Young, H. Lebrette, V. Srinivas, A. S. Brewster, T. Michels-Clark, J. A. Clinger, B. Andi, M. Ibrahim, E. Pastor, C. de Lichtenberg, R. Hussein, C. J. Pollock, M. Zhang, C. A. Stan, T. Kroll, T. Fransson, C. Weninger, M. Kubin, P. Aller, L. Lassalle, P. Brauer, M. D. Miller, M. Amin, S. Koroidov, C. G. Roessler, M. Allaire, R. G. Sierra, P. T. Docker, J. M. Glownia, S. Nelson, J. E. Koglin, D. Zhu, M. Chollet, S. Song, H. Lemke, M. Liang, D. Sokaras, R. Alonso-Mori, A. Zouni, J. Messinger, U. Bergmann, A. K. Boal, J. M. Bollinger Jr., C. Krebs, M. Hogbom, G. N. Phillips Jr., R. D. Vierstra, N. K. Sauter, A. M. Orville, J. Kern, V. K. Yachandra and J. Yano, *Nat. Methods*, 2017, **14**, 443–449.
88. S. Tsujino and T. Tomizaki, *Sci. Rep.*, 2016, **6**, 25558.
89. H. P. Stevenson, D. P. DePonte, A. M. Makhov, J. F. Conway, O. B. Zeldin, S. Boutet, G. Calero and A. E. Cohen, *Philos. Trans. R. Soc. London*, 2014, **369**, 20130322.
90. F. Stellato, D. Oberthür, M. Liang, R. Bean, C. Gati, O. Yefanov, A. Barty, A. Burkhardt, P. Fischer, L. Galli, R. A. Kirian, J. Meyer, S. Panneerselvam, C. H. Yoon, F. Chervinskii, E. Speller, T. A. White, C. Betzel, A. Meents and H. N. Chapman, *IUCrJ*, 2014, **1**, 204–212.
91. A. Y. Lyubimov, T. D. Murray, A. Koehl, *I. E.* Araci, M. Uervirojnangkoorn, O. B. Zeldin, A. E. Cohen, S. M. Soltis, E. L. Baxter, A. S. Brewster, N. K. Sauter, A. T. Brunger and J. M. Berger, *Acta Crystallogr., Sect. D: Biol. Crystallogr.*, 2015, **71**, 928–940.
92. R. G. Sierra, C. Gati, H. Laksmono, E. H. Dao, S. Gul, F. Fuller, J. Kern, R. Chatterjee, M. Ibrahim, A. S. Brewster, I. D. Young, T. Michels-Clark, A. Aquila, M. Liang, M. S. Hunter, J. E. Koglin, S. Boutet, E. A. Junco, B. Hayes, M. J. Bogan, C. Y. Hampton, E. V. Puglisi, N. K. Sauter, C. A. Stan, A. Zouni, J. Yano, V. K. Yachandra, S. M. Soltis, J. D. Puglisi and H. DeMirci, *Nat. Methods*, 2015, **13**, 59–62.

93. R. G. Sierra, H. Laksmono, J. Kern, R. Tran, J. Hattne, R. Alonso-Mori, B. Lassalle-Kaiser, C. Glöckner, J. Hellmich, D. W. Schafer, N. Echols, R. J. Gildea, R. W. Grosse-Kunstleve, J. Sellberg, T. A. McQueen, A. R. Fry, M. M. Messerschmidt, A. Miahnahri, M. M. Seibert, C. Y. Hampton, D. Starodub, N. D. Loh, D. Sokaras, T.-C. Weng, P. H. Zwart, P. Glatzel, D. Milathianaki, W. E. White, P. D. Adams, G. J. Williams, S. Boutet, A. Zouni, J. Messinger, N. K. Sauter, U. Bergmann, J. Yano, V. K. Yachandra and M. J. Bogan, *Acta Crystallogr., Sect. D: Biol. Crystallogr.*, 2012, **68**, 1584–1587.
94. P. Nogly, V. Panneels, G. Nelson, C. Gati, T. Kimura, C. Milne, D. Milathianaki, M. Kubo, W. Wu, C. Conrad, J. Coe, R. Bean, Y. Zhao, P. Båth, R. Dods, R. Harimoorthy, K. R. Beyerlein, J. Rheinberger, D. James, D. DePonte, C. Li, L. Sala, G. J. Williams, M. S. Hunter, J. E. Koglin, P. Berntsen, E. Nango, S. Iwata, H. N. Chapman, P. Fromme, M. Frank, R. Abela, S. Boutet, A. Barty, T. A. White, U. Weierstall, J. Spence, R. Neutze, G. Schertler and J. Standfuss, *Nat. Commun.*, 2016, **7**, 12314.
95. S. Botha, K. Nass, T. R. Barends, W. Kabsch, B. Latz, F. Dworkowski, L. Foucar, E. Panepucci, M. Wang, R. L. Shoeman, I. Schlichting and R. B. Doak, *Acta Crystallogr., Sect. D: Biol. Crystallogr.*, 2015, **71**, 387–397.
96. U. Weierstall, *Philos. Trans. R. Soc. London*, 2014, **369**, 20130337.
97. M. Boudes, D. Garriga, A. Fryga, T. Caradoc-Davies and F. Coulibaly, *Acta Crystallogr., D: Struct. Biol.*, 2016, **72**, 576–585.
98. K. R. Beyerlein, D. Dierksmeyer, V. Mariani, M. Kuhn, I. Sarrou, A. Ottaviano, S. Awel, J. Knoska, S. Fuglerud, O. Jönsson, S. Stern, M. O. Wiedorn, O. Yefanov, L. Adriano, R. Bean, A. Burkhardt, P. Fischer, M. Heymann, D. A. Horke, K. E. J. Jungnickel, E. Kovaleva, O. Lorbeer, M. Metz, J. Meyer, A. Morgan, K. Pande, S. Panneerselvam, C. Seuring, A. Tolstikova, J. Lieske, S. Aplin, M. Roessle, T. A. White, H. N. Chapman, A. Meents and D. Oberthuer, *IUCrJ*, 2017, **4**, 769–777.